Initial conditions for retrospective predictions

Deliverable 2.2

Authors: Bernardello R., Bopp L., Ilyina T., Li H., Mignot J., Mosneron-Dupin C., Ortega P. and Tourigny E.

This project received funding from the Horizon 2020 programme under the grant agreement No. 821003.

Document Information

GRANT AGREEMENT	821003
PROJECT TITLE	Climate Carbon Interactions in the Current Century
PROJECT ACRONYM	4C
PROJECT START DATE	2019-06-01
RELATED WORK PACKAGE	WP2
RELATED TASK(S)	T2.2
LEAD ORGANISATION	ENS
AUTHORS	Bernardello R., Bopp L., Ilyina T., Li H., Mignot J., Mosneron-Dupin C., Ortega P. & Tourigny E.
SUBMISSION DATE	2020-09-30
DISSEMINATION LEVEL	Public

History

DATE	SUBMITTED BY	REVIEWED BY	VISION (NOTES)
2020-09-28	Bernardello R. et al	Leo de Sousa-Webb & Pierre Friedlingstein	Minor improvements and formatting
2020-09-29	4C Executive Board members	Bernardello R. et al	Scanning and feedback
2020-09-28	Leo de Sousa-Webb & Pierre Friedlingstein	Bernardello R. et al	Minor formatting, proofreading and accessibility checks

Please cite this report as: Bernardello R. et al. (2020), Initial conditions for retrospective predictions, D2.2 of the 4C project

Table of Contents

1 Methodological aspects of initialisation in 4C Earth System Models 6

1.1 IPSL-CM6A-LR 7

1.2 MPI-ESM1.2-HR 8

1.3 EC-Earth3-CC 9

2 Evaluation of ocean-atmosphere and land-atmosphere carbon fluxes in the initialisation simulations 11

3 Additional initialised simulations as performed with the 4C Earth System Models 13

3.1 IPSL-CM6A-LR 13

3.2 MPI-ESM1.2-LR 15

3.3 EC-Earth3-CC 16

4 Conclusions 19

5 References 20

List of tables

Table 1: Overview of 4C prediction systems and initialisation techniques. 6

Table 2: Configurations tested to produce the ocean reconstructions with EC-Earth3. 16

List of figures

Figure 1: Time series of the global anomalous CO2 flux relative to the climatological mean in each modeling system into the ocean (left) and land (right) from reconstruction / initialisation (top) and uninitialised simulations (bottom). The long-term linear trends are removed for all the time-series. Left panels include available observation-based estimates from SOM-FFN (Landschutzer et al. 2016). Numbers on the legends show the correlations relative to GCB2019 and correlations relative to SOM-FFN data-based estimates of the CO2 flux into the ocean (shown in brackets). (Figure is redrawn based on Ilyina et al. submitted to GRL, updated with output from EC-Earth3). 12

Figure 2: Time series of the global CO2 flux into the ocean in various configurations of the IPSL-CM6A-LR climate model as compared to an ocean-forced simulation with NEMO-PISCES and to various data-based estimates. The black line shows the data-based estimate, resulting from the average of the MPI-SOMFFN (Landschutzer et al. 2016), Jena-MLS (Roedenbeck et al. 2014) and CMEMS (Denvil-Sommer et al. 2019) products. The grey shading indicates the maximum and minimum value reached by these three data sets at each time step. The blue curve shows the average of the three standard assimilation runs performed at IPSL for the DCPP project, and also used in Ilyina et al. (subm). The red curve shows the average of three new assimilation runs performed at IPSL with an alternative assimilation procedure (see text). The green curve shows the average the 3 historical simulations (uninitialised). The black-dash line shows the ocean forced simulation with NEMO-PISCES used for the Global Carbon Budget 2019 (Friedlingstein et al. 2019). 14

Figure 3: Time series of atmospheric carbon increment (left), net carbon flux into the ocean (middle) and the land (right) from MPI-ESM1.2 emission-driven assimilation together with the global carbon budget (GCB2019) data. The GCB2019 carbon fluxes are from multi-model ocean and land stand-alone simulations; the thick blue curves show multi-model mean and the thin blue curves show individual model results. The numbers in legend show correlation coefficients between assimilation and GCB2019. 15

Figure 4: Validation of surface chlorophyll in ocean reconstructions using MODIS-Aqua. Here is shown the example of the Equatorial Pacific region. Experiment a1z8 with a no-nudging band between 15°S-15°N and a different vertical 3D nudging profile showed overall the best performance..... 17

Figure 5: Anomaly Correlation Coefficient (ACC) of SST in two November initialised seasonal forecast system based on EC-Earth3. ACC values are computed against EN4 observations (Good et al. 2013). The two figures refer to two tests performed using ORAS5 as the reference product for the ocean data assimilation in the generation of ocean initial conditions. The dramatic loss of predictive skill over the North Atlantic is visible as a region of negative correlation southeast of the Labrador Sea area. 18

About 4C

Climate-Carbon Interactions in the Current Century (4C) is an EU-funded H2020 project that addresses the crucial knowledge gap in the climate sensitivity to carbon dioxide emissions, by reducing the uncertainty in our quantitative understanding of carbon-climate interactions and feedbacks. This will be achieved through innovative integration of models and observations, providing new constraints on modelled carbon-climate interactions and climate projections, and supporting Intergovernmental Panel on Climate Change (IPCC) assessments and policy objectives.

Executive Summary

The objective of WP2 of 4C is to develop the capability of 3 European ESMs (IPSL-ESM, MPI-ESM, EC-Earth) to predict the near-term evolution of carbon sinks, atmospheric CO2, and climate in response to future emissions. To do so, IPSL-ENS, MPG and BSC have produced reconstructions of the recent past that will be used as initial conditions for retrospective near-term predictions. This deliverable (1) describes the standard procedures adopted by each group to initialise their coupled climate-carbon simulations over the last decades, (2) presents a brief evaluation of the reconstructed ocean-atmosphere and land-atmosphere fluxes against data-based estimates, and (3) summarises some of the alternative or improved initialisation techniques on which the modelling groups are still working.

Keywords

Earth System Models, Initialization, Carbon fluxes reconstructions

1 Methodological aspects of initialisation in 4C Earth System Models

As detailed in Ilyina et al. (subm.), we recall here the main technical aspects of the initialisation techniques or data assimilation methods that have been used by the 4C climate modelling groups (Table 1). Following the DCPP philosophy, i.e. not specifying a unique technique for initialising the prediction model systems, these techniques strongly differ among the 4C groups.

Note, however, that in all model systems, the carbon cycle components are only indirectly initialised with initialisation/assimilation techniques directly affecting the physical variables of the Earth System Models. Note also that all simulations discussed here are all forced by imposed atmospheric concentrations and land-use changes over the historical period.

Table 1: Overview of 4C prediction systems and initialisation techniques.

MODEL	IPSL-CM6A-LR	MPI-ESM1.2-HR	EC-EARTH3-CC
Resolution Atmosphere	2.5°x1.3°, 79 levels	T127, 95 levels	T255, 91 levels
Resolution Ocean	1°, 75 levels	0.4, 40 levels	1°, 75 levels
Initialisation Atmosphere	N/A	ERA-40 and ERAInterim: Vorticity, divergence, log(p), T; full field	ERA-Interim/ERA5 Full field
Initialisation Ocean	EN4 SST and Atlantic SSS anomalies	ORAS4 3D T-S anomalies, sea-ice concentration anomalies from NSIDC	Reconstruction nudged to ORAS4 T-S using the same 3D nudging protocol as in Sanchez-Gomez et al (2016) Full field
Ensemble Size			10 members
References	Boucher et al. (2020)	Mauritsen et al. (2019)	Sanchez-Gomez et al (2016)

1.1 IPSL-CM6A-LR

Retrospective predictions based on the IPSL-CM6A-LR climate model are initialised from a global century-long simulation in which anomalies of global EN4 sea surface temperature and Atlantic sea surface salinity presented by Reverdin et al. (2019) have been nudged into the climate model. The nudging procedure is described by Estella-Perez et al. (2020).

It includes, in particular, a variable nudging strength depending on the upper mixed layer depth, as described in Ortega et al. 2016. Furthermore, the low-frequency modulation of sea surface salinity anomalies as reconstructed by Reverdin et al. (2019) are combined to the climatology of SSS from EN4.

There is no assimilation of subsurface ocean, sea ice, biogeochemistry or atmospheric observations. Note that two flavours of this initialisation procedure have been tested, and described further down in section 4. 3 assimilation simulations, starting from 3 different historical simulations, have been integrated from 1900 to 2016. The initialised retrospective predictions are launched from only 1 member.

1.2 MPI-ESM1.2-HR

MPI-ESM1.2-HR retrospective predictions are initialised from a separate reconstruction/assimilation run, in which observation and reanalysis data are nudged into the Earth system model (Li et al. 2019, Pohlmann et al. 2019, Ilyina et al. 2020).

HR refers to high resolution with atmosphere ~100km in the horizontal and 95 vertical levels and ocean ~40km in horizontal and 40 vertical levels. We nudge atmospheric 3D full-field temperature, vorticity, divergence, and surface pressure from the European Centre for Medium-Range Weather Forecasts (ECMWF) Re-Analysis ERA40 (Uppala et al. 2005) for the period 1958-1979 and ERA-Interim (Dee et al. 2011) for the period from 1980-2018. For the ocean component, anomalous 3D temperature and salinity from the ECMWF Ocean Reanalysis System 4 (ORAS4) (Balmaseda et al. 2013) and sea-ice concentration from the National Snow and Ice Data Center (NSIDC) satellite observations (as described in Bunzel et al. 2016) are nudged.

The sea-ice concentration is a combination of a climatology before 1979 without satellite data and anomalies from 1979 when satellite observations are available. This assimilation run is under CMIP6 forcings with prescribed atmospheric CO2 concentration. As the ocean biogeochemical processes adjust to the assimilated physical climate states slowly, we perform a pre-assimilation of about 50 years. Each year of assimilation starts from November to October in the next year, and the restart files on October 31st are saved yearly for initialised retrospective prediction runs.

1.3 EC-Earth3-CC

Initial conditions (ICs) for retrospective predictions with EC-Earth3-CC are obtained from three different procedures for ocean, land vegetation and atmosphere. For the ocean, the procedure includes restoring of SST and SSS as well as 3D temperature and salinity Newtonian dumping below the mixed layer. We use the restoring timescale distribution of Sanchez-Gomez et al. (2016). At the surface SST is restored using a feedback coefficient between flux and temperature of -40 W/m2/K while the feedback parameter for freshwater fluxes is set at -167 mm/day. Below the mixed layer, the restoring timescale varies between 10 days (up to 800m) and 360 days (below 800m). The reference dataset used for surface restoring and 3D nudging is the ECMWF Ocean Reanalysis System 4 (ORAS4) (Balmaseda et al. 2013), while the atmospheric forcing used is the DRAKKAR forcing set DFS5.2 (Dussin et al. 2016) which is based on the ERA-40 and Era-Interim reanalyses. As in Sanchez-Gomez et al. (2016), we decided to use a configuration that leaves a no-nudging band between 15ºS-15ºN. Sea Ice, as well as ocean biogeochemistry, are let free to evolve in response to the constrained ocean physics.

The atmospheric initial conditions are obtained from the ERA5 (or ERA-Interim) reanalysis from ECMWF, which have been interpolated to the EC-Earth3 Standard Resolution configuration of T255/N128 in the horizontal and 91 vertical levels, using full-pos from openIFS cycle 40r1.

The land vegetation ICs are done using the EC-Earth LSM (Land Surface Model) forced by reanalysis datasets. The EC-Earth LSM couples the OSM (Offline Surface Model), an offline version of H-TESSEL which is the land surface component of the IFS (Integrated Forecast System), to the LPJ-Guess dynamic vegetation model. This coupling has been done to facilitate development and testing of the coupling between IFS/H-TESSEL and LPJ-Guess and also to perform observationally-forced reconstructions in which the partitioning of land surface fluxes and albedo are consistent with the fully-coupled model. The EC-Earth LSM uses the same CMIP6 forcings for land-use, nitrogen and greenhouse gases as the coupled ESM version EC-Earth-CC, thus allowing it to perform PI (Pre-industrial) spinups and historical simulations up to the present day. The LPJ-Guess version used in EC-Earth-CC model has been improved for C4MIP to smooth the fluxes to the atmosphere and also for 4C to be able to start/stop the model in any date of the calendar year, which is necessary to produce ICs on Nov. 1st required for decadal predictions.

The atmospheric forcing used is the ERA-20C reanalysis for the period prior to 1979 and ERA-Interim/ERA5 from 1979-2018, for consistency with the ORAS4/ORAS5 ocean reanalyses used for generating the Ocean ICs. The use of bias-corrected reanalyses such as GSWP3 for the period prior to 1979 is currently being investigated, as the transition from ERA-20C to ERA-Interim/ERA5 forcings in 1979 generates a shift in carbon stock and NPP/GPP compared to a reconstruction with only ERA-20C The official land vegetation initial conditions produced for 4C have been done using ERA-Interim, and an alternate dataset has been produced using ERA5 forcings, which will be used to initialise near-term predictions in Task 2.4.

The procedure used to generate the ICs is as follows:

1. LPJG offline spinup of 500 years with constant 1850 CMIP6 forcings and repeating 1901-1910 atmospheric forcings which have been processed by the OSM.

2. OSM+LPJG run with transient CMIP6 forcings from 1850-1901 by repeating the 1901-1920 atmospheric forcings, following the TRENDY protocol.

3. Continue the transient run up to 1979, saving the LPJ-Guess restarts on Nov. 1st and Jan. 1st from 1950 onwards.

4. Perform a similar transient run from 1979-present day using ERA-Interim/ERA5 forcings.

2 Evaluation of ocean-atmosphere and land-atmosphere carbon fluxes in the initialisation simulations

Here we assess the variability of the ocean-atmosphere and land-atmosphere carbon fluxes (hereafter referred to as carbon sinks) by comparing the simulated fluxes from the reconstruction/assimilation simulations to observatio-based estimates and to the carbon sinks estimates from the global carbon budget (Friedlingstein et al. 2019) over the last decades (1982-2013; Fig. 1).

These reconstructed sinks for initialisation are also compared to the simulated sinks from classical historical simulations (hereafter referred to as uninitialised) following CMIP6 forcing in which the model physics evolves freely (and does not match necessarily the observed variability). The reconstructions capture multi-year variations of the carbon sinks as represented by the SOM-FFN observation-based estimates of the ocean carbon sink (Landschützer et al. 2015) and the carbon sinks from the global carbon budget (GCB2019, Friedlingstein et al. 2019).

The uninitialised historical simulations show much smaller variations as they mainly capture the trends of carbon sinks in response to rising carbon emissions. The results from 4C models together with other models suggest that the reconstructions, in which the observations are assimilated into the Earth system models, outperform the uninitialised historical simulations in capturing multi-year variations of the ocean and land carbon sinks. Therefore, the reconstructions will be used for initialising the retrospective predictions.

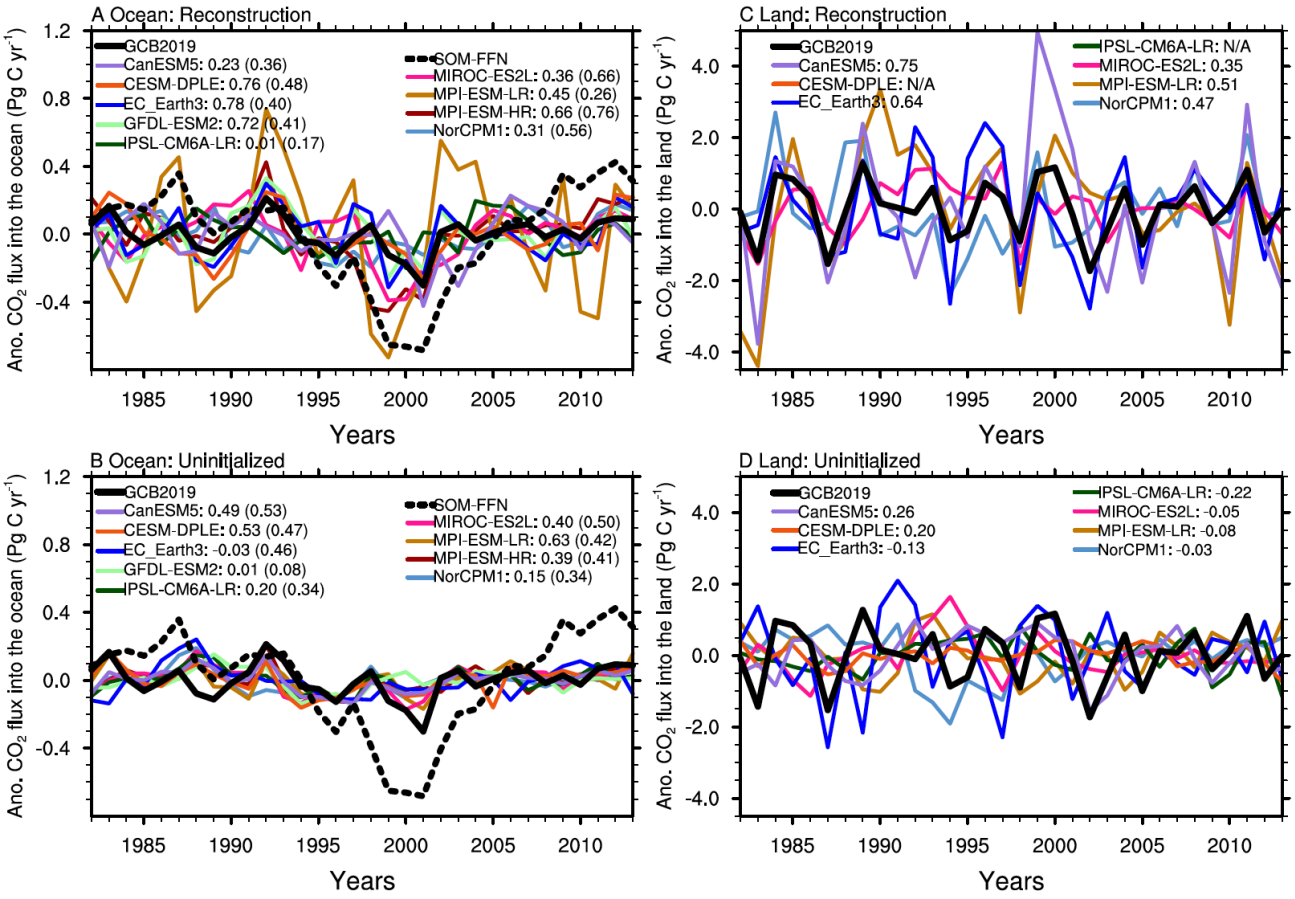

Figure 1: Time series of the global anomalous CO2 flux relative to the climatological mean in each modeling system into the ocean (left) and land (right) from reconstruction / initialisation (top) and uninitialised simulations (bottom). The long-term linear trends are removed for all the time-series. Left panels include available observation-based estimates from SOM-FFN (Landschutzer et al. 2016). Numbers on the legends show the correlations relative to GCB2019 and correlations relative to SOM-FFN data-based estimates of the CO2 flux into the ocean (shown in brackets). (Figure is redrawn based on Ilyina et al. submitted to GRL, updated with output from EC-Earth3).

3 Additional initialised simulations as performed with the 4C Earth System Models

3.1 IPSL-CM6A-LR

The preliminary analysis of initial conditions in IPSL-CM6A-LR highlighted the fact that salinity variability is particularly high (and probably overestimated) in IPSL-CM6A-LR, while it is damped due to a 3-yrs running filtering process in the SSS dataset. This discrepancy may have induced a damping of the model's variability and therefore led to artificially smooth reconstructions (old-assim), at least in terms of large scale oceanic circulation, and in particular Atlantic overturning circulation (AMOC).

For this reason, IPSL/ENS group is currently working on an updated version (new assim) of the reconstruction methodology in which the low-frequency variability of the salinity data used for the nudging has been inflated to better fit the model's internal variability. Figure 2 shows the reconstruction of the globally averaged CO2 flux into the ocean over the 20th century in both assimilation ensemble means (3 members), as well as non-initialised historical simulations and reconstructed observations (MPM).

This figure confirms that both assimilation simulations are relatively consistent among each other, at least over the early part of the century. They also show some signs of synchronisation with the observations, although with a strongly underestimated variance. Yet even forced oceanic simulations do not achieve to reproduce the observed variance.

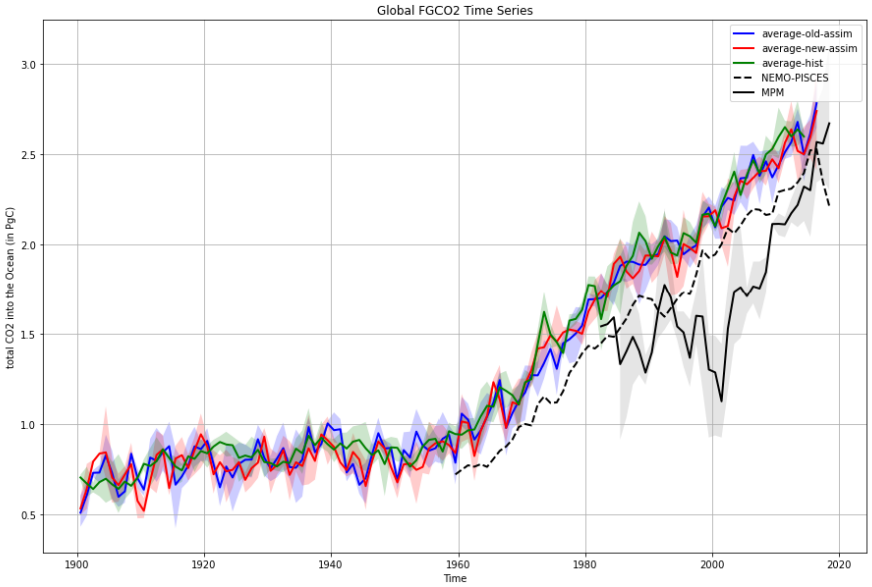

Figure 2: Time series of the global CO2 flux into the ocean in various configurations of the IPSL-CM6A-LR climate model as compared to an ocean-forced simulation with NEMO-PISCES and to various data-based estimates. The black line shows the data-based estimate, resulting from the average of the MPI-SOMFFN (Landschutzer et al. 2016), Jena-MLS (Roedenbeck et al. 2014) and CMEMS (Denvil-Sommer et al. 2019) products. The grey shading indicates the maximum and minimum value reached by these three data sets at each time step. The blue curve shows the average of the three standard assimilation runs performed at IPSL for the DCPP project, and also used in Ilyina et al. (subm). The red curve shows the average of three new assimilation runs performed at IPSL with an alternative assimilation procedure (see text). The green curve shows the average the 3 historical simulations (uninitialised). The black-dash line shows the ocean forced simulation with NEMO-PISCES used for the Global Carbon Budget 2019 (Friedlingstein et al. 2019).

3.2 MPI-ESM1.2-LR

In addition to the MPI-ESM1.2-HR assimilation with prescribed atmospheric CO2 concentration forcing, for the first time, we perform assimilation with prognostic atmospheric CO2 under emission-driven configuration. This is based on MPI-ESM1.2-LR. LR refers to low resolution with atmosphere ~200km in horizontal and 47 vertical levels and ocean ~150km in horizontal and 40 vertical levels. The new framework of emission-driven simulations with interactive carbon cycle enables reconstruction and predictions of atmospheric CO2 concentration.

The nudging schemes are the same as the assimilation with prescribed atmospheric CO2 concentration. In this assimilation, we leave out ocean nudging for the equatorial band of 5S-5N to avoid spurious upwelling there due to nudging. New features are the CO2 emission forcing and the interactive carbon cycle. Our first results from the assimilation show comparable evolution of the atmospheric carbon increment and carbon fluxes with the GCB2019 (Fig. 3).

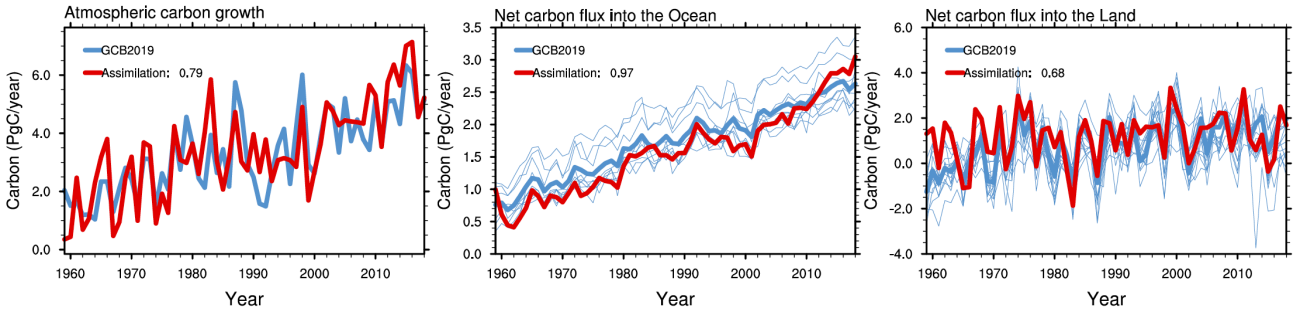

Figure 3: Time series of atmospheric carbon increment (left), net carbon flux into the ocean (middle) and the land (right) from MPI-ESM1.2 emission-driven assimilation together with the global carbon budget (GCB2019) data. The GCB2019 carbon fluxes are from multi-model ocean and land stand-alone simulations; the thick blue curves show multi-model mean and the thin blue curves show individual model results. The numbers in legend show correlation coefficients between assimilation and GCB2019.

3.3 EC-Earth3-CC

For the ocean initial conditions, we tested several combinations of spatial distribution and strength of the 3D nudging using ECMWF Ocean Reanalysis System 4 (ORAS4) as our reference dataset. A latitudinal band with no 3D nudging was included in all cases to avoid spurious vertical velocities and instabilities at low latitudes as in Sanchez-Gomez et al. (2016; Table 2).

Table 2: Configurations tested to produce the ocean reconstructions with EC-Earth3.

Experiment	3D nudging T&S	Surface restoring (SST&SSS)	No 3D nudging
a1yp (baseline configuration in EC-Earth3.3)	Default: τ (z=1.5m) = 3 days τ (z=14m) = 3.1 days τ (z=61m) = 3.2 days τ (z=180m) = 3.8 days τ (z=500m) = 5.6 days τ (z=950m) = 9.2 days τ (z=1390m) = 15.4 days τ (z=3000m) = 84 days τ (z=4900m) = 329 days	Default: γ_T = -40 W/m2/K γ_S = -167 mm/day	3°S-3°N
a1z8 (to test the impact of the vertical profile for the 3D nudging)	τ(M.L. < z < 800m) = 10 days τ(z > 800m) = 360 days Same as in Sanchez-Gomez et al (2016)	Default	15°S-15°N
a1z2 (to test the impact of surface nudging)	Default	γ_T = -600 W/m2/K γ_S = -2250 mm/day	3°S-3°N
a20w (to test the impact of the buffer zone without 3D nudging)	Default	Default	6.4°S-6.4°N

To validate these tests, we used remote sensing surface chlorophyll in various regions of the ocean (Fig. 4).

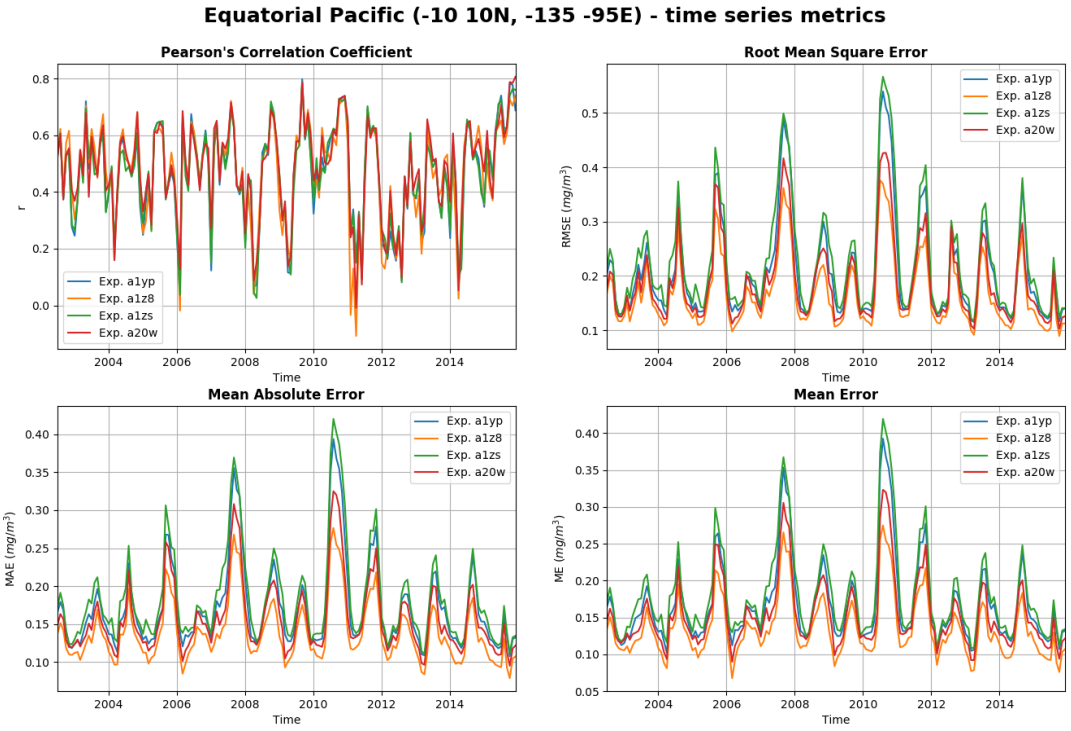

Figure 4: Validation of surface chlorophyll in ocean reconstructions using MODIS-Aqua. Here is shown the example of the Equatorial Pacific region. Experiment a1z8 with a no-nudging band between 15ºS-15ºN and a different vertical 3D nudging profile showed overall the best performance.

These reconstructions, however, cannot be used for the envisaged retrospective decadal predictions because ORAS4 has been discontinued and replaced by the new Ocean Reanalysis System 5 (ORAS5) which is maintained and updated. For this reason, to keep our prediction modelling system working, we had to modify our procedure so it can assimilate ORAS5 (which is produced at a higher horizontal and vertical resolution than ORAS4 and EC-Earth3-CC). However, ORAS5 presents significant differences from ORAS4, in particular a problematic non-stationary bias over the North Atlantic, causing a loss of skill over this region in the fifth operational version of ECMWF's seasonal prediction system (Tietsche et al., 2020). A problem that also affects two EC-Earth seasonal predictions initialised from ORAS5-based reconstructions (Fig. 5) and that is expected to degrade the skill of the decadal predictions if the same approaches are used.

To overcome this problem, we started performing extensive tests using ORAS5 as well as other observation-based products to identify the best configuration (surface restoring and 3D nudging strength/distribution) to circumvent the non-stationary bias problem. At the moment, three strategies have been selected because of their encouraging preliminary results:

1- Nudging towards ORAS5 at the surface (as Tietsche et al., 2020 demonstrates that the non-stationarity bias is linked to the subsurface) and towards EN4 (Good et al., 2013) in the subsurface.

2- The same as the previous one, but using two datasets for the subsurface nudging: EN4 in a box extending from the Labrador Sea to the Grand Banks, and ORAS5 elsewhere.

3- Reconstruction reproducing the OMIP2 protocol but including surface nudging of SST towards COBE-SST (Hirahara et al., 2014; the same product used to produce the JRA55 reanalysis, which is used as the atmospheric forcing).

Tests (2) and (3) have been completed and are now being analysed while test (1) is ongoing.

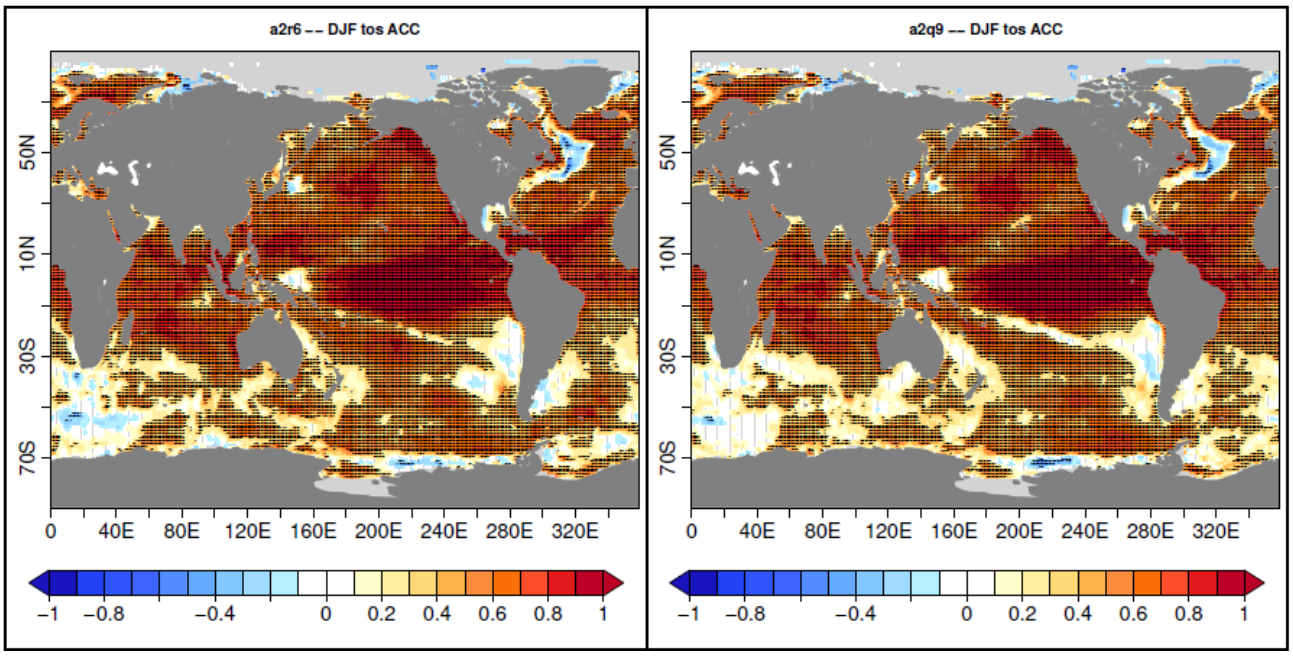

Figure 5: Anomaly Correlation Coefficient (ACC) of SST in two November initialised seasonal forecast system based on EC-Earth3. ACC values are computed against EN4 observations (Good et al. 2013). The two figures refer to two tests performed using ORAS5 as the reference product for the ocean data assimilation in the generation of ocean initial conditions. The dramatic loss of predictive skill over the North Atlantic is visible as a region of negative correlation southeast of the Labrador Sea area.

4 Conclusions

The initialisation simulations performed with the standard versions of the 4C earth system models (IPSL-CM, MPI-ESM and EC-Earth) show interesting performances when compared to estimates based on observations of oceanic and biospheric carbon sinks. In particular, this comparison reveals that these reconstructions outperform the uninitialised historical simulations in capturing multi-year variations.

These models are therefore used subsequently for producing retrospective predictions (Ilyina et al. subm) to estimate the possibilities of CO_2 prediction within a few years.

In parallel, several avenues are explored to improve the score of the initialised simulations (modifications of the assimilation procedure, use of other data sets) – these avenues will be further exploited in the coming months. A first evaluation of an initialisation simulation with a forced-emission model for which the simulated atmospheric CO_2 growth rate can be directly compared to observations is also presented with very promising scores.

5 References

Balmaseda, M. A., K. Mogensen, A. T. Weaver (2013). Evaluation of the ECMWF ocean reanalysis system ORAS4. Q. J. R. Meteorol. Soc. 139, 1132–1161.

Bunzel, F., Notz, D., Baehr, J., Müller, W. A., & Fröhlich, K. (2016). Seasonal climate forecasts significantly affected by observational uncertainty of Arctic sea ice concentration. *Geophysical Research Letters*, 43, 852–859. doi.org/10.1002/2015GL066928

Dee, D.P., S. M. Uppala, A. J. Simmons, P. Berrisford, P. Poli, S. Kobayashi, U. Andrae, M. A. Balmaseda, G. Balsamo, P. Bauer, P. Bechtold, A. C. M. Beljaars, L. van de Berg, J. Bidlot, N. Bormann, C. Delsol, R. Dragani, M. Fuentes, A. J. Geer, L. Haimberger, S. B. Healy, H. Hersbach, E. V. Hólm, L. Isaksen, P. Kållberg, M. Köhler, M. Matricardi, A. P. McNally, B. M. Monge-Sanz, J.-J. Morcrette, B.-K. Park, C. Peubey, P. de Rosnay, C. Tavolato, J.-N. Thépaut, F. Vitart (2011), The ERA-Interim reanalysis: configuration and performance of the data assimilation system. Q. J. R. Meteorol. Soc. 137, 553–597.

Dussin, R., B. Barnier and L. Brodeau (2016), Up-dated description of the DFS5 forcing data set: The making of Drakkar forcing set DFS5. DRAKKAR/MyOcean Report 01-04-16, LGGE, Grenoble, France.

Estella Perez, V.; Mignot, J.; Guilyardi, E.; Swingedouw, D.; Reverdin, G. Advances in Reconstructing the AMOC using Sea Surface Observations of Salinity, *Clim Dyn* 55, 975–992 (2020). doi.org/10.1007/s00382-020-05304-4

Friedlingstein, P., Jones, M., O'sullivan, M., Andrew, R., Hauck, J., Peters, G., et al. (2019). Global carbon budget 2019. Earth System Science Data, 11 (4), 1783-1838.

Good, S. A., M. J. Martin and N. A. Rayner, 2013. EN4: quality controlled ocean temperature and salinity profiles and monthly objective analyses with uncertainty estimates, Journal of Geophysical Research: Oceans, 118, 6704-6716, doi:10.1002/2013JC009067

Hirahara, Shoji, Masayoshi Ishii, Yoshikazu Fukuda, 2014: Centennial-Scale Sea Surface Temperature Analysis and Its Uncertainty. J. Climate, 27, 57–75.

Ilyina, T., H. Li, A. Spring, W. A. Muller, L. Bopp, M. O. Chikamoto, G. Danabasoglu, M. Dobrynin, J. Dunne, F. Fransner, P. Friedlingstein, W. Lee, N. S. Lovenduski, W.J. Merryeld, J. Mignot, J.Y. Park, R. Seferian, R. Sospedra-Alfonso, M. Watanabe, S. Yeager (2020), Predictable variations of the carbon sinks and atmospheric CO2 growth in a multi-model framework, *Geophysical Research Letters*, in review.

Kobayashi, S., Ota, Y., Harada, Y., Ebita, A., Moriya, M., Onoda, H., Onogi, K., Kamahori, H., Kobayashi, C., Endo, H., Miyaoka, K., and Takahashi, K.: The JRA-55 reanalysis: general specifications and basic characteristics, J. Meteorol. Soc. Jpn., 93, 5–48, doi.org/10.2151/jmsj.2015-001, 2015.

Landschützer, P., Gruber, N., Haumann, F. A., Rodenbeck, C., Bakker, D. C., Van Heuven, S., et al. (2015). The reinvigoration of the southern ocean carbon sink. *Science*, 349 (6253), 1221-1224.

Li, H., Ilyina, T., Muller, W. A., & Landschutzer, P. (2019). Predicting the variable ocean carbon sink. *Science advances*, 5 (4), eaav6471.

Ortega P., Guilyardi E., Swingedouw D., Mignot J**.**, Nguyen S. Reconstructing extreme AMOC events through nudging of the ocean surface: A perfect model approach. *Climate Dynamics*, doi.org/10.1007/s00382-017-3521-4

Pohlmann, H., W. A. Müller, M. Bittner, S. Hettrich, K. Modali, K. Pankatz, J. Marotzke, 2019: Realistic quasi-biennial oscillation variability in historical and decadal hindcast simulations using CMIP6 forcing. *Geophys. Res. Lett.*, 46, 14118-14125 doi:10.1029/2019GL084878

Reverdin, G., Friedman, A.R., Chafik, L. *et al.* North Atlantic extratropical and subpolar gyre variability during the last 120 years: a gridded dataset of surface temperature, salinity, and density. Part 1: dataset validation and RMS variability. *Ocean Dynamics* **69,** 385–403 (2019). doi.org/10.1007/s10236-018-1240-y

Sanchez-Gomez, E., Cassou, C., Ruprich-Robert, Y. et al. Drift dynamics in a coupled model initialised for decadal forecasts. Clim Dyn 46, 1819–1840 (2016). doi.org/10.1007/s00382-015-2678-y

Tietsche, S., Balmaseda, M., Zuo, H. et al. The importance of North Atlantic Ocean transports for seasonal forecasts. Clim Dyn 55, 1995–2011 (2020). doi.org/10.1007/s00382-020-05364-6

Uppala, S. M., P. W. KÅllberg, A. J. Simmons, U. Andrae, V. Da Costa Bechtold, M. Fiorino, J. K. Gibson, J. Haseler, A. Hernandez, G. A. Kelly, X. Li, K. Onogi, S. Saarinen, N. Sokka, R. P. Allan, E. Andersson, K. Arpe, M. A. Balmaseda, A. C. M. Beljaars, L. Van De Berg, J. Bidlot, N. Bormann, S. Caires, F. Chevallier, A. Dethof, M. Dragosavac, M. Fisher, M. Fuentes, S. Hagemann, E. Hólm, B. J. Hoskins, L. Isaksen, P. A. E. M. Janssen, R. Jenne, A. P. Mcnally, J.-F. Mahfouf, J.-J. Morcrette, N. A. Rayner, R. W. Saunders, P. Simon, A. Sterl, K. E. Trenberth, A. Untch, D. Vasiljevic, P. Viterbo, J. Woollen (2005), The ERA-40 re-analysis. Q. J. R. Meteorol. Soc 131, 2961–3012.